UCID- 17111

Lawrence Livermore Laboratory

A FEASIBILITY STUDY FOR USE OF A GERMANIUM DETECTOR IN THE LOFT GAMMA-RAY DENSITOMETER

S. P. Swierkowski

April 27, 1976

Prepared for U.S. Energy Research & Development Administration under contract No. W-7405-Eng-48.

DISCLAIMER

April 22, 1976

A Feasibility Study for Use of a Germanium Detector in the LOFT Gamma-Ray Densitometer*

S. P. Swierkowski

Introduction

This work report is part of the above titled study for Aerojet Nuclear Company (purchase order S-6238, 11/19/75). The primary aim of this study is to predict the performance of a gamma-ray densitometer system using computer modeling techniques. The system consists of a collimated ^{137}Cs source, a pipe containing a variable amount of water absorber, and a shielded and collimated germanium detector system. An idealized model of this system is shown in Figure 1 with the sources described in Table 1; these are also described in the Work Statement of 10/2/75. The gamma-ray energy spectrum (number of photon counts as a function of energy) has been computed for several sources at the detector. The response for combined source configurations has been obtained by linear superposition. The signal essentially consists of the counts in an energy window centered on the ^{137}Cs source at 662 keV that originate from this source. The noise is the background counts in the signal energy window that originate from ^{16}N scatter radiation and direct and shield tank activation gammas. The detector signal has been computed for 0, 50, and 100% water in the pipe.

Some basic questions addressed by this study are: Will a germanium detector in this scheme work? Is the lower resolution of NaI detectors sufficient to make them work? What are the signal and total detector count rates? What is the detector gamma-ray spectrum? What is the

*This work was performed under the auspices of the U.S. Energy Research and Development Administration under contract number W-7405-ENG-48.

sampling time required for a few percent accuracy on the average density in the pipe? What other detector application requirements (e.g., packaging and reliability) are critical? How should one adjust design parameters such as collimater diameter, source location and energy, etc. to optimize the performance?

Problem Description and Computational Geometry

The photon-electron transport code, SANDYL, used in this study has some constraints built into its available geometry descriptors. One is constrained to use orthogonal X, Y, and Z planes and generalized conics to describe the boundaries of the geometrical zones; in addition, all circular cylinders must be parallel to the Z axis. To readily accomodate these constraints, the problem geometry of Figure 1 was modified as shown in Figure 2 while retaining the critical features. The critical features are the spatial distribution of material near the Z axis. Thus the collimation angles, source-to-detector distance, steel walls, and water path are unchanged.

The usual scheme in detector modeling with SANDYL is to first run SANDYL for a specific geometry with a detector present. SANDYL can produce a variety of output such as geometry plots, photon or electron flux versus energy plots, photon or electron flux versus angle, energy and electron deposition edits, etc.; it can also produce a file, ELOSTFILE, containing the energy depositions and the zone locations for each incident primary photon. A second Monte-Carlo code called MOZART uses the energy deposition track information in ELOSTFILE and forms the detector spectrum including electronics noise and other detector artifacts that distort the absorbed energy spectrum. MOZART produces energy spectra for the

incident photon flux, the absorbed photons, and the final detector instrument spectrum.

Since the fraction of unscattered ^{137}Cs photons through both walls of the stainless steel (SS304 was used) pipe was less than 1% with the pipe only filled with air, it is computationally impractical to make one long computer run that would provide a statistically significant number of counts in the detector. The problem was broken down into several parts for this reason and this also aids in checking the results and debugging the runs. Intermediate transmitted photon fractions and their spectra (when smoothed) can then be used as input for the next stage of computation.

Summary of Major SANDYL Runs

A brief outline of major SANDYL runs will now be given; the development of the complete model will be explained and major computation features and approximations will be described. The actual SANDYL output for these runs is contained on the approximately 500 pages of microfiche labeled ANC Ø3-Ø8, and ANC Ø9-12, 16, 18. The runs to be discussed are listed in Table 2. The angle A in Table 2 refers to the angular limit in the photon source; the angle A is between the reference direction axis and the maximum angular deviation of a source photon from this axis. In other words, the angular distribution is uniform within a cone with angle 2A. The number F_x^y is the number of photons entering zone x within energy group y normalized by the number of source photons; this is not the true fraction for a real source because the solid angle of the conic has not yet been folded in. This data has been taken from the microfiche output.

Runs 2-4 are preliminary runs primarily for setup and debug. They employ a series of Pb "detectors" on the back side of a stainless steel wall;

the geometry is shown in Figure 3.

Runs 5-9 are full geometry runs with a ^{137}Cs source. Run 5 shows the geometry effects with transparent steel ($\rho = 10^{-5}$ gm/cm^3) and the pipe fluid is air. Runs 7-9 are with SS304 walls and water in the pipe with densities of 0.0, 0.5, and 1.0 gm/cm^3. Run 8, for example, shows that $\bar{F}_1^{31} = 4.79 \times 10^{-4}$ where the water density is 1 gm/cm^3. The solid angle of the source is:

$$\Omega_s = 2\pi(1 - \cos A), \text{ steradians} \qquad (1)$$

For run 8, $\Omega_s = 0.002533$ steradians. The true fraction of group 31 (650-750 keV) photons entering the detector (zone 1) is 9.66×10^{-8} photons per source photon; these represent approximately the number of full-energy unscattered ^{137}Cs photons entering the detector. The angle $A = 1.627°$ is a minimal value chosen to maximize the SANDYL efficiency and is based on geometrical limits sketched in worksheet ANC Ø8 in the Appendix. The SANDYL geometry raw worksheets are shown in the Appendix. They are not as clear as the figures but do contain all the zone, plane, and conic numbers and other descriptive information.

Runs 10-13 are full geometry runs similar to runs 5-9 except that the source is ^{16}N; actually, a simplified ^{16}N source with emission at only 6130 keV is used with emission from a central core of water. The detector contribution from this source is expected to be slightly lower than actual because it excludes scatter from the outer core of water and backscatter from the inner core. With more computer time, this could have been done more accurately.

Run 14 moves the source up to a location inside the first wall at 0.1 inches from the inside wall of the pipe. This run demonstrates a substantial improvement could be obtained if one wall of the pipe were eliminated for the ^{137}Cs source. Collimation of the ^{137}Cs source is not necessary for two reasons. First, indirect scattered radiation from the source will be reduced in energy and not in the full energy signal window. Two, the detector is geometrically collimated as well as energy selective so only water absorbtion along the detector collimation axis will be significant.

Run 16 simulates a 2 MeV source beamed down the pipe. It demonstrates negligible scattering into the detector. Run 19 simulates the shielding problem for three NaI detectors on one side of 3 inches of lead shielding with a 0-10 MeV source beamed against the other side. This run indicates the count rate in group 31 (650-750 keV) is 4.6×10^5 γ/sec and the total count rate is 1.38×10^7 γ/sec. This is for a 2 inch thick, 2 inch diameter NaI detector and the source was 0-10 MeV, 1×10^7 γ/cm^2/sec from the shield tank. This run shows that 3 inches of lead shielding produces an unacceptably high count rate for a 2 x 2 NaI detector; 4 or 5 inches of lead shielding may be required to reduce the background from this source. Using a 1 x 1 NaI detector instead of a 2 x 2 would reduce this background by a factor of 4 while the ^{137}Cs peak detection efficiency would only drop about 30%; the full NaI detector is subject to the shield tank gammas while only the collimated portion of the detector is subject to the ^{137}Cs gammas.

Spectral Results and Count Rate Data

If the shield tank gammas are shielded to a level well below that of the ^{16}N background, then the only significant sources are the ^{16}N and the

^{137}Cs. With this assumption, the detector spectrum has been simulated for two cases. The first case employs a Ge detector as shown in Figure 2 and worksketch ANC Ø5; a worst case of 4 keV FWHM noise was imposed on the Ge detector and the spectral results are shown in Figures 5-7. The two sources present are ^{16}N at 137 $\mu Ci/cm^3$ at 100% water (1 gm/cm^3) in the pipe in zone 8 and a 30 Ci ^{137}Cs source distributed evenly over a 1/2 inch diameter disk as shown in Figure 2. The sample time was 0.25 seconds. The ^{137}Cs photopeak at 662 keV clearly is evident in Figure 7. The flat characteristic in the background around and above the Cs peak makes a simple background subtraction process possible. If this is done, it is clear that a detector with less resolution may also do the job, since it is the integrated counts over the energy windows that measure the signal and background. Since time limits did not allow re-running the codes to simulate a NaI detector, an approximate simulation was obtained by using the germanium absorbtion data with the noise of NaI (8% = 53 keV FWHM) imposed and the results are shown in Figures 8-10. Actual NaI performance should be better than this because the detector would be bigger and have a higher Z. With the collimation of the detector, this will imply a higher photopeak efficiency than germanium and a higher peak-to-Compton ratio.

By integrating portions of the spectrum in Figure 7 the counts in various energy windows are given in Table 3. A very simple background subtraction using the average of an adjacent upper and lower pair of windows shows that the signal-to-noise ratio is roughly 25 for a worst-case germanium detector. Considering, for an approximate comparison, the pseudo NaI case from Figure 10, a similar analysis is indicated in Table 4 and the pseudo NaI signal-to-noise is roughly 17. The count rates for these two cases are summarized in Table 5. The total detector count rate should

not exceed 10^5 counts/second. The detector collimation of Figure 2 should be reduced slightly to avoid detector and electronics overload. If the detector collimater were reduced from 3/4 to 1/2 inch, this should suffice without reducing the signal-to-noise too much; this would also have the advantage of reducing the diameter of the core of water whose average density is being measured.

Summary of Results and Future Work

The densitometer as previously described and analyzed should work for both germanium and NaI as the detector. The question of reliability and complexity of design and application for the two detector types is more complex. Neutron damage on germanium must be considered and it is not clear by guestimate whether germanium can survive long enough. In addition, the LN cooling and vacuum cryostat requirements of germanium will pose more difficult packaging and design requirements. On the other hand, the resolution and signal-to-noise for germanium is somewhat better than NaI. The pseudo-NaI calculation shows that it should be possible to measure the water density at ρ = 1 gm/cm^3 to about 6% accuracy in 0.25 seconds. These results are for a homogeneous water-steam mixture in the pipe. Inhomogeneous situations would have to be done with multiple detectors.

It appears that large significant gains could be made by using a source sealed and attached to the inside wall of the pipe; for the source, transmission through one pipe wall would be eliminated. The ^{137}Cs signal would increase by approximately ten by doing this.

There are several possibilities for future work. One could redo the present calculations for a NaI detector. A higher energy source could

also be considered (^{60}Co 1.17 MeV + 1.33 MeV). A more accurate geometry could be used with off-axis sampling paths. A possible SANDYL geometry for this arrangement is shown in Figure 11.

TABLE 1

Gamma Ray Sources for Computer Modeling

1. 30 Ci ^{137}Cs collimated source 662 keV.

2. ^{16}N 6-7 MeV 137 $\mu Ci/cm^3$ at 100% water.
   Normal operation and blowdown.

3. Neutron activation gammas from shield tank.
   0-10 MeV 1 x 10^7 $\gamma/cm^2/sec$. Normal operation
   and blowdown.

4. Delayed gammas from core scattered once into pipe.
   0-2 MeV 5 x 10^7 $\gamma/cm^2 sec$. Inside pipe blowdown.

TABLE 2 Major SANDYL Runs

Run No.	Geometry & options	Results	Energy, keV	Counts
3	SS304 wall 1.4 inch thick	$\bar{F}_1^{31}$ = 1.88E-2	662	4 x 1K
	Pb detectors 1-3	$\bar{F}_2^{31}$ = 2.33E-2		
	coll, det 1 = 0.5 in. dia.	$\bar{F}_3^{31}$ = 0.0		
	A = 7.125°			
4	Same as 3 except	F_1^{31} = 3.20E-3	662	1 x 2.5K
	Pb det 1 = 0.1841 in. dia.	F_2^{31} = 1.68E-2		
	coll = 0.5 in. dia.	F_3^{31} = 2.40E-2		
5	Full geometry (Fig. 2)	$\bar{F}_1^{31}$ = 0.355	662	4 x 1K
	A = 1.627°	$\bar{F}_1^{T}$ = 0.370		
	SS304 = $\rho = 10^{-5}$	(T = TOTAL FLUX)		
	fluid = air			
6	Full geometry, A = 1.627°		662	4 x 5K
	Air in pipe			
	SS304 = ρ = 8.03 gm/cm^3			

TABLE 2 Major SANDYL Runs, cont.

Run No.	Geometry & options	Results	Energy, keV	Counts
7	Same as 6 but more counts ρ = 0.0 H_2O	$\bar{F}_1^{31}$ = 5.90E-3 $\bar{F}_1^{T}$ = 6.08E-2	662	3 x 15K + 1 x 30K
8	Same as 6, 7 but ρ = 1.0 H_2O	$\bar{F}_1^{31}$ = 4.79E-4 $\bar{F}_1^{T}$ = 5.18E-4	662	4 x 15K
9	Same as 6, 7, 8 but ρ = 0.5 H_2O	$\bar{F}_1^{31}$ = 1.94E-3 $\bar{F}_1^{T}$ = 1.985E-3	662	4 x 15K
10	Full geometry A = 45° ^{16}N source in zone 8 4 in. dia. ρ = 1.00 H_2O	$\bar{F}_1^{46}$ = 2.60E-4 $\bar{F}_1^{T}$ = 5.40E-4	6130	4 x 15K
11	Same as 10 but more counts group 46 (5.62-6.49 MeV)	$\bar{F}_1^{46}$ = 2.46E-4 $\bar{F}_1^{T}$ = 4.42E-4	6130	4 x 75K

TABLE 2 Major SANDYL Runs, cont.

Run No.	Geometry & options	Results	Energy, keV	Counts
12	Same as 10 but zone 8 is smaller 1 in. dia. A = 3.066°	F_1^{46} = 7.57E-3 F_1^T = 8.60E-3	6130	1 x 30K
13	Same as 10 but A = 45° ρ = 0.50 H_2O		6130	4 x 75K
16	Full geometry like 11 but 2 MeV down pipe source ρ = 1.00 H_2O	F_1^T negligible	2000	4 x 1K
18	Same as 3-wall shield, but NaI detectors		0-10 MeV uniform	2500 + 595 + 10 x 2

TABLE 3

Simple Spectral Analysis for Ge (FWHM = 4 keV)

Detector (Figure 7) with Sample Time = 0.25 seconds

	Energy Window, keV	Counts
$^{137}Cs \pm 4$ keV	658-666	739
	666-746	535
	578-658	384

$S + B = 739$

$B^* = 45.95$

$S = 693.05$

$S/\sigma_T = 24.73$

$\sigma_1 = \sqrt{739} = 27.18$

$\sigma_2 = \sqrt{45.9} = 6.77$

$\sigma_T = 28.02$

*Background obtained as average from upper and lower adjacent windows.

TABLE 4

Simple Spectral Analysis for Ge (FWHM = 53 keV) -

Pseudo-NaI Detector (Figure 10) with Sample Time = 0.25 seconds

	Energy Window, keV	Counts
$^{137}Cs \pm 50$ keV	612-712	1158
	712-812	460
	812-912	433
	912-1012	353
	1012-1112	324

$S + B = 1158$

$B^* = 480$

$S = 678$

$S/\sigma_T = 16.75$

$\sigma_1 = \sqrt{1158} = 34.03$

$\sigma_2 = \sqrt{480} = 21.91$

$\sigma_T = 40.47$

*Background obtained by extrapolating upper energy windows.

TABLE 5

Detector Count Rates for the Spectra of Figure 7 and 10.

	Count rate, photons/sec
Ge FWHM = 4 keV	
Cs peak signal	2772
Signal window 658-666 keV	2956
Total detector	116612
Ge FWHM = 53 keV	
Cs peak signal	2712
Signal window 612-712 keV	4632
Total detector	116612

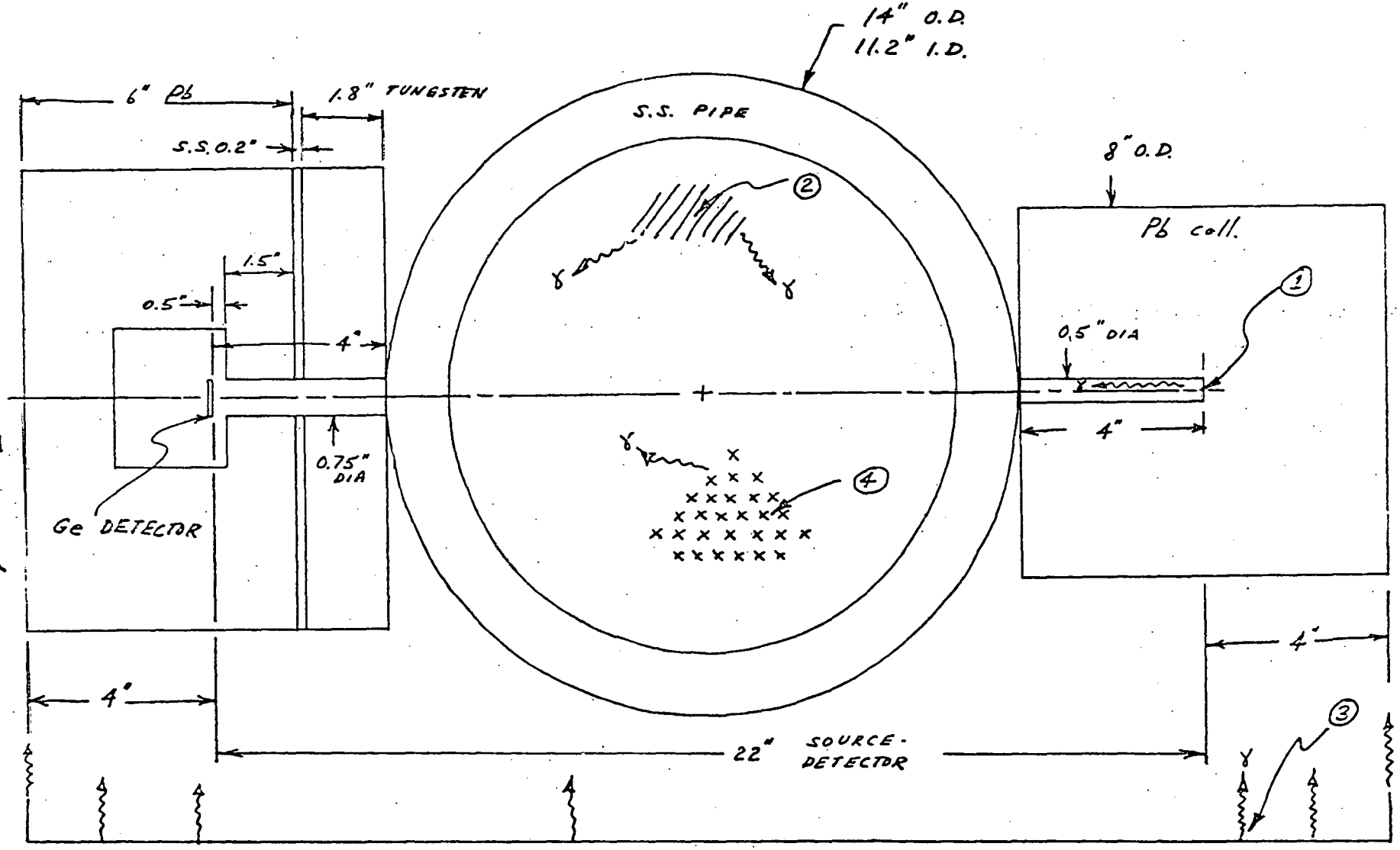
14" O.D.
11.2" I.D.
6" Pb
1.8" TUNGSTEN
S.S. 0.2"
S.S. PIPE
8" O.D.
Pb coll.
1.5"
0.5"
4"
0.5" DIA
0.75" DIA
Ge DETECTOR
4"
4"
4"
22" SOURCE-DETECTOR
γ
1
2
3
4

Figure 1.

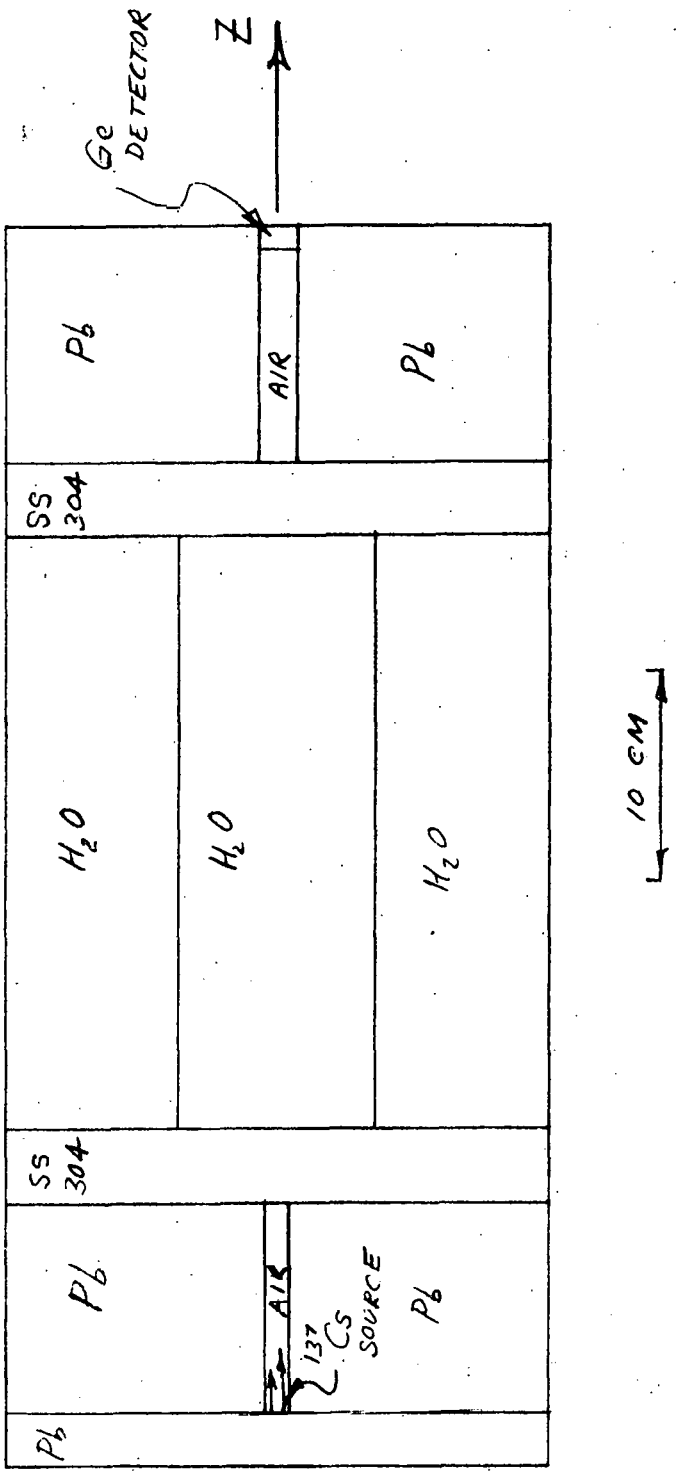

Figure 2. Full geometry used in computations. Cylindrically symmetric. Used in runs ANC 5-16. Also see appendix sketch.

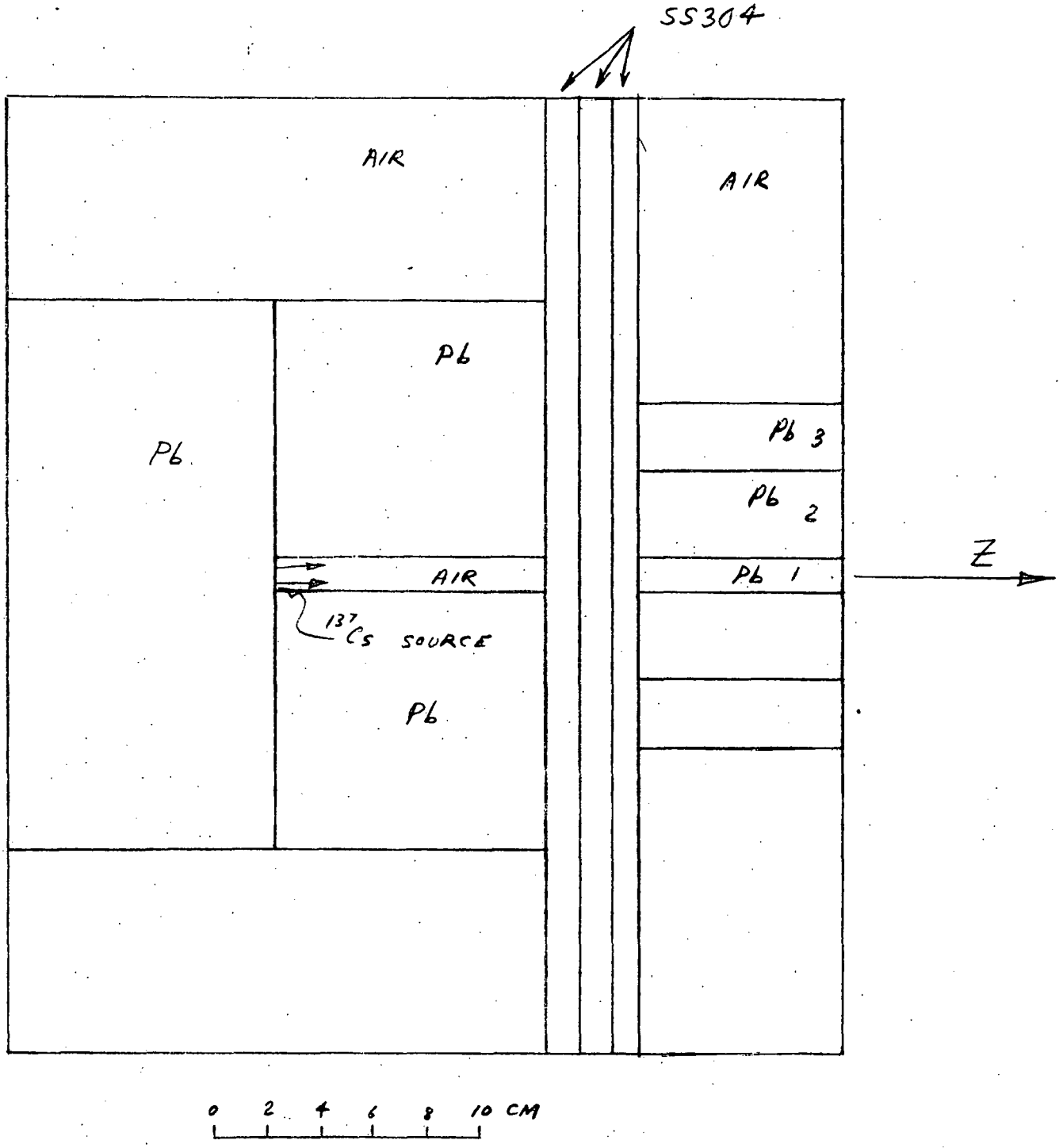

Figure 3. SANDYL geometry used in runs ANC 2-4. Cylindrically symmetric.

(Deleted)

Figure 4

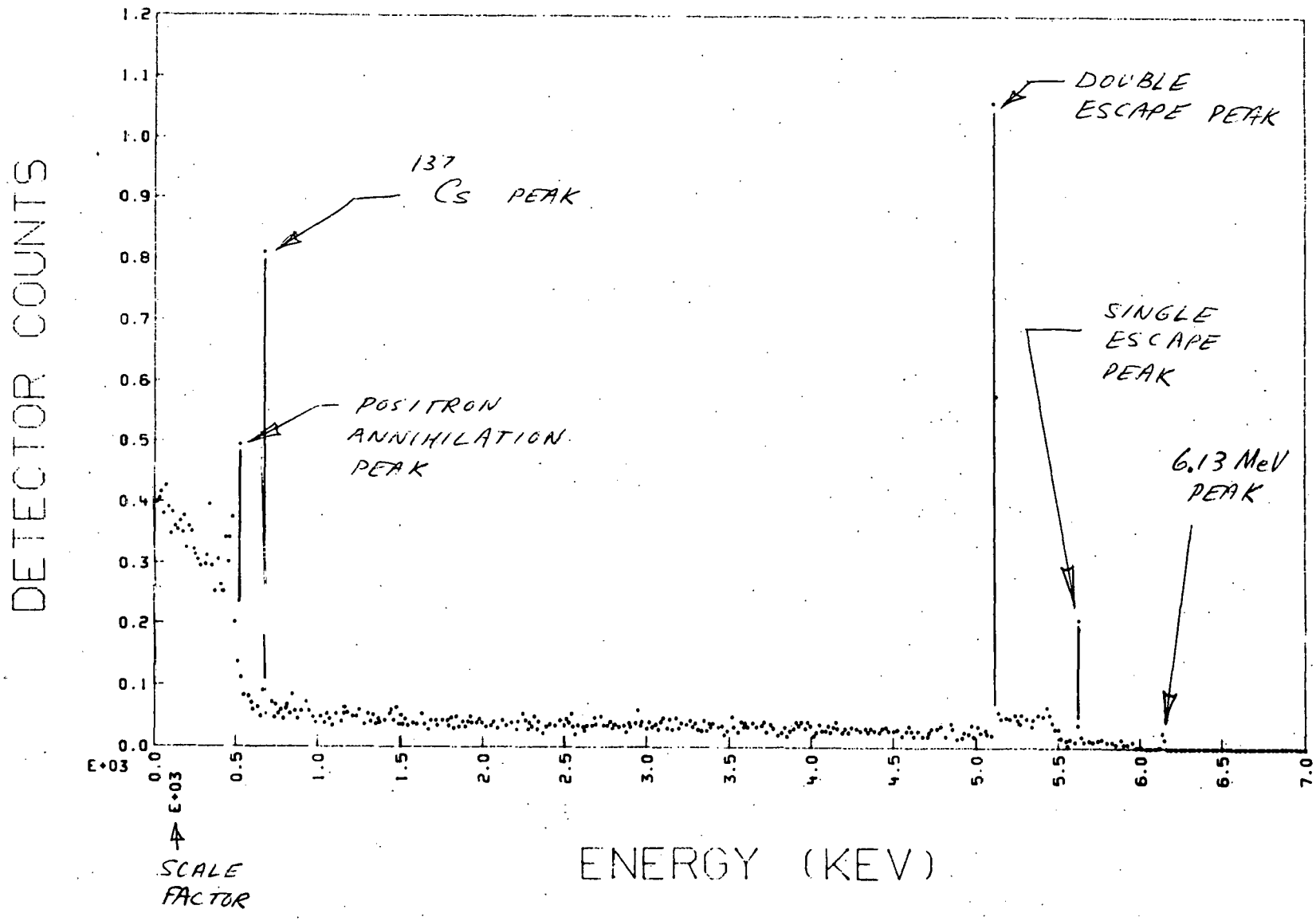

Figure 5.

03 3/5/76 662KEV+N16 ANC11,08 H20=1.00

CTS= 162684 INS= 2176 MIX= 26977 ALL= 159815

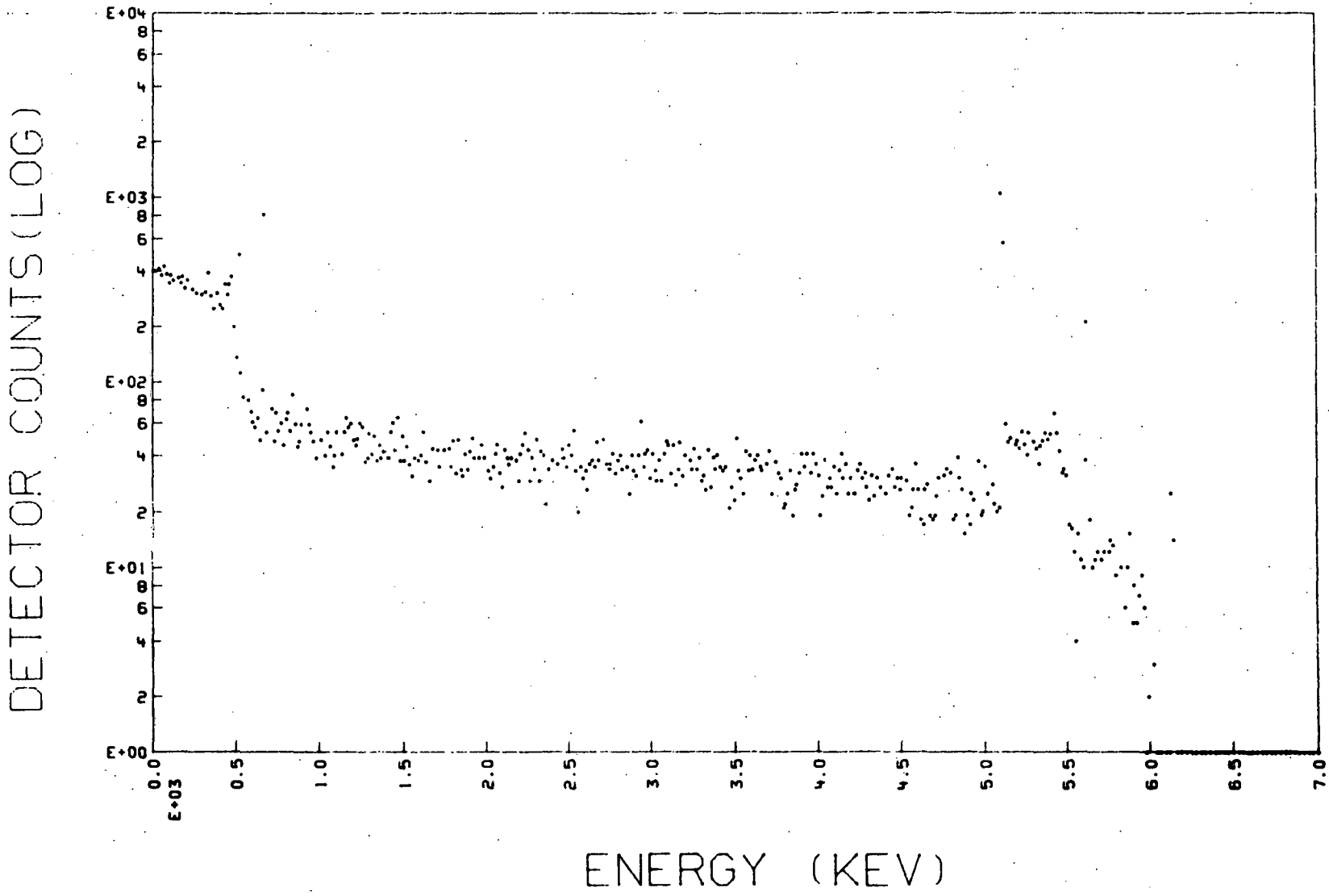

Fig. 5 (Log plot of Fig. 5)

03 3/5/76 662KEV+N16 ANC11,08 H20=1.00

CTS= 162684 INS= 2176 MIX= 26977 ALL= 159815

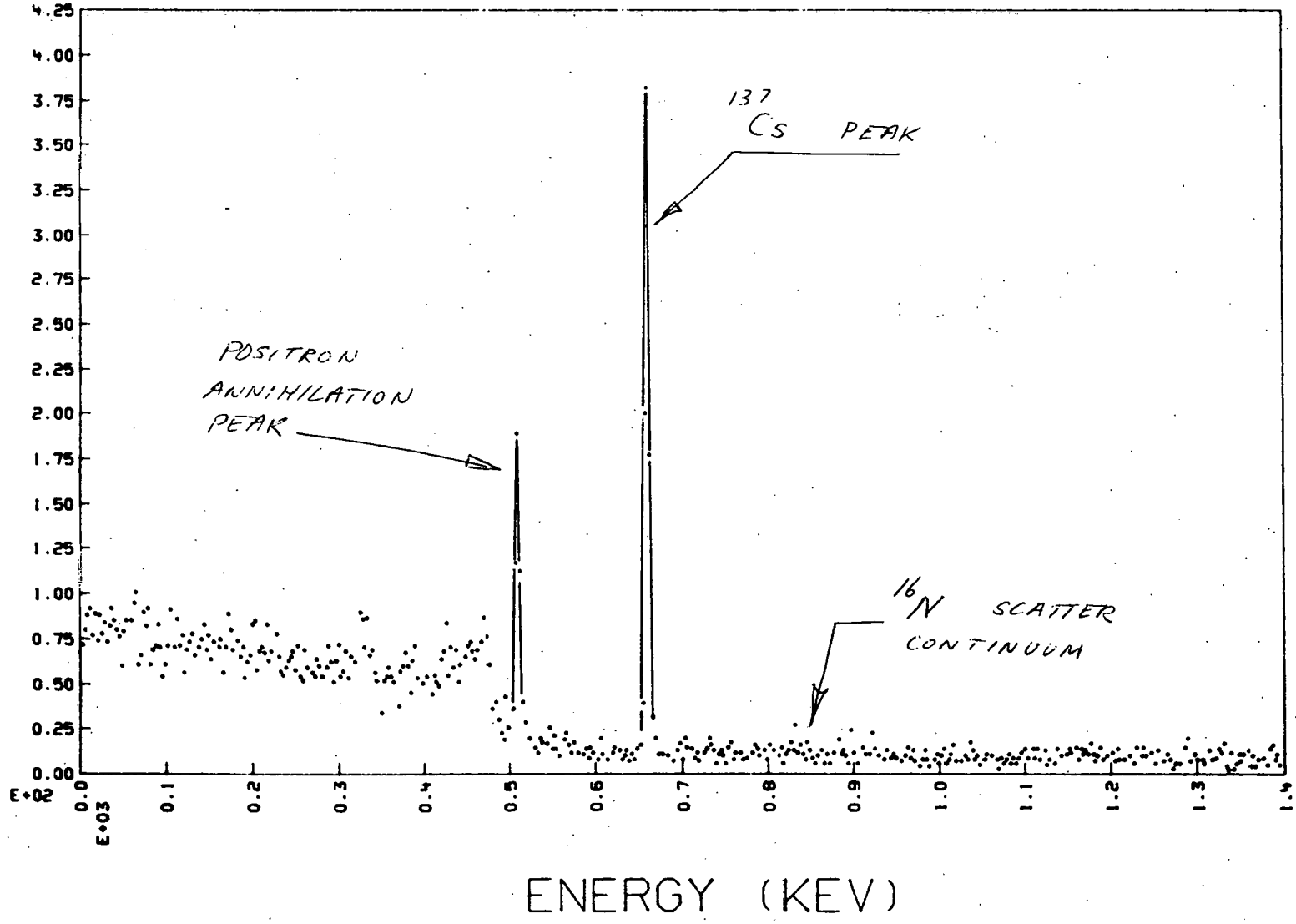

03 3/5/76 662KEV+N16 ANC11,08
739 CTS,KEV 658.0 666.0
EV/CH=2800.0

Figure 7. (Expanded plot of Fig 5.)

Figure 8

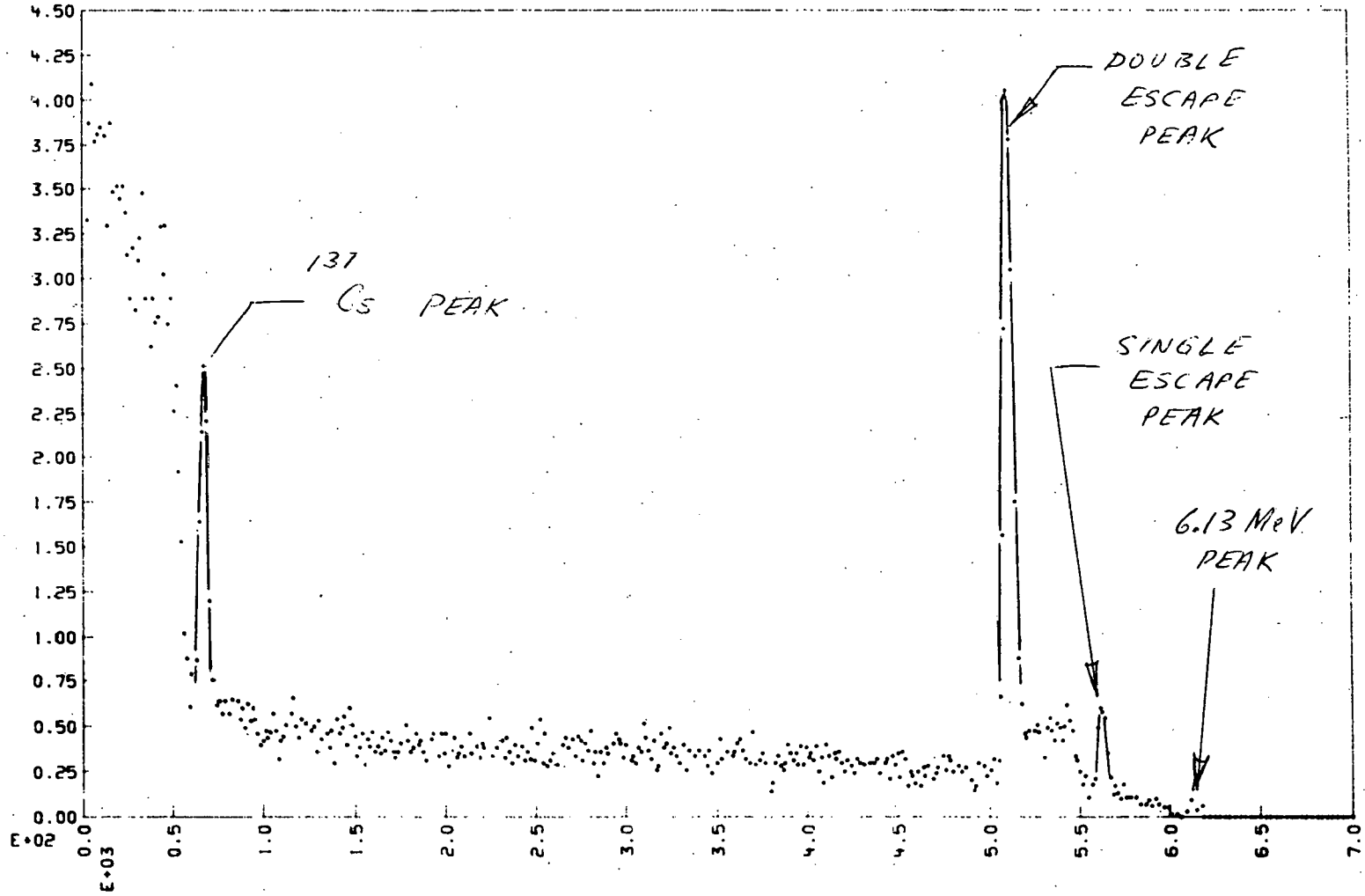

04 3/17/76 662KEV+N16 ANC11.08 H20=1.00

CTS= 162684 INS= 2176 MIX= 26977 ALL= 159815

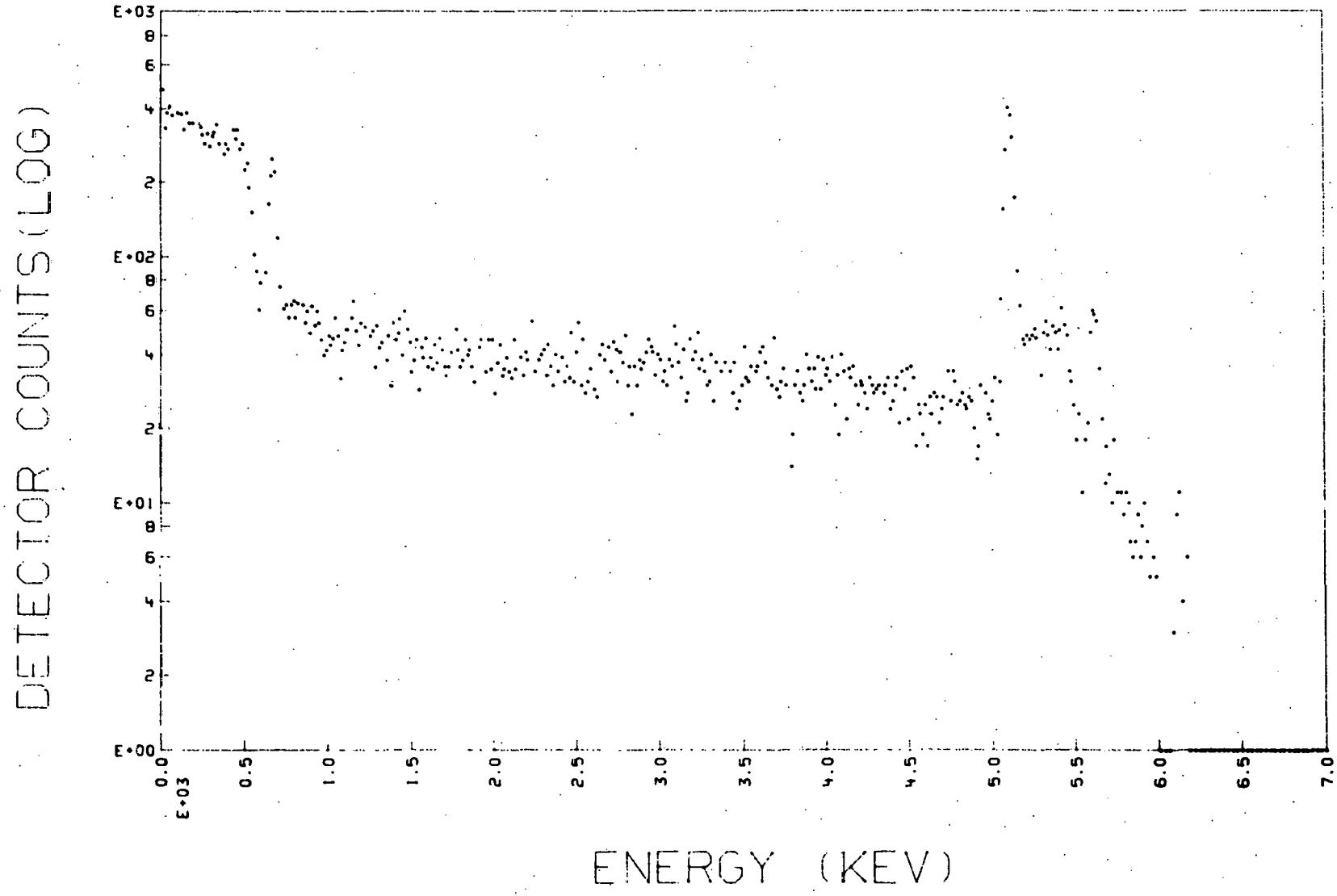

Figure 9. Log plot of Fig 8)

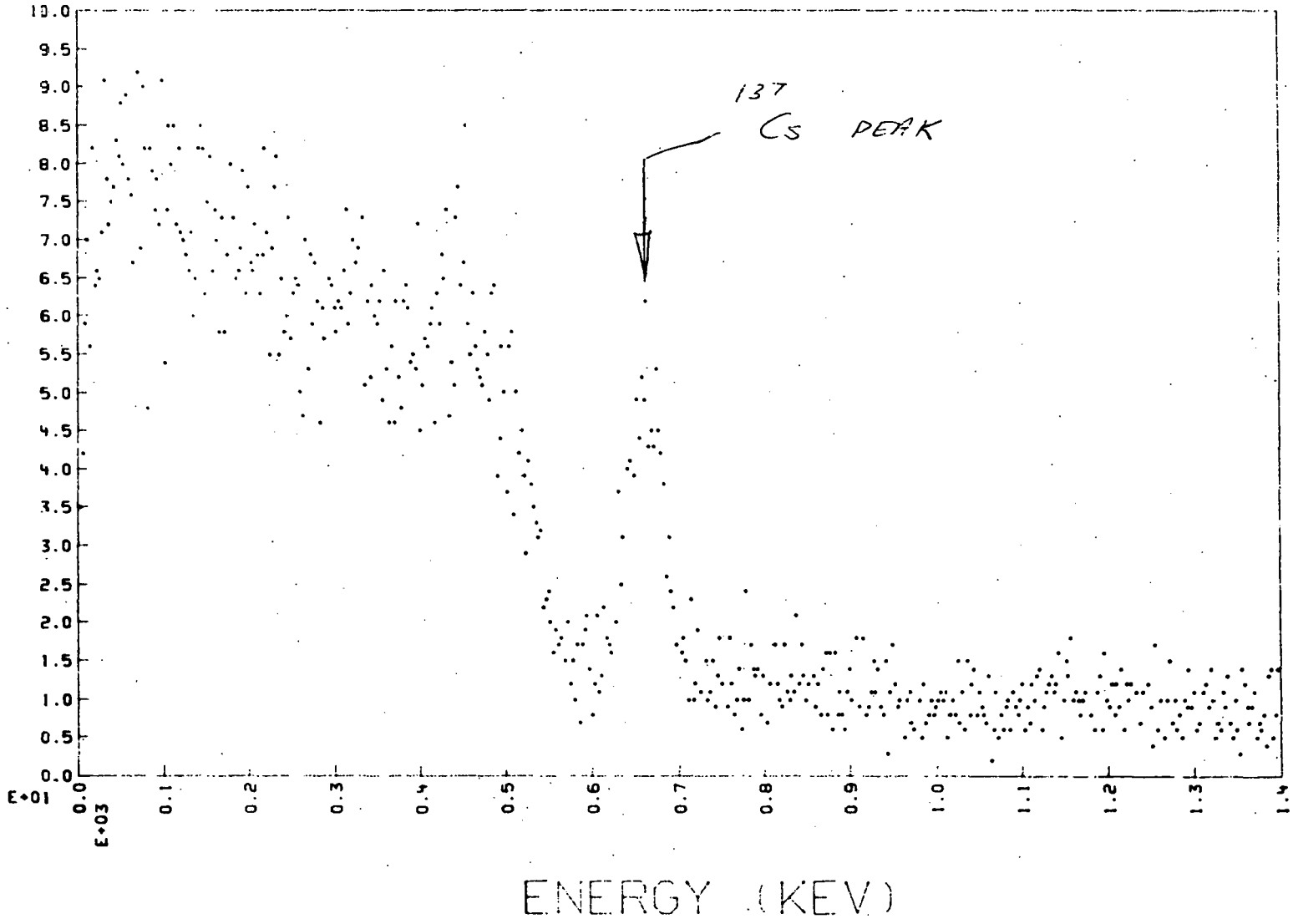

04 3/17/76 662KEV+N16 ANC11,08
1158 CTS,KEV 612.0 712.0
EV. CH=2800.0

Figure 10. (Expanded plot of Fig. 9)

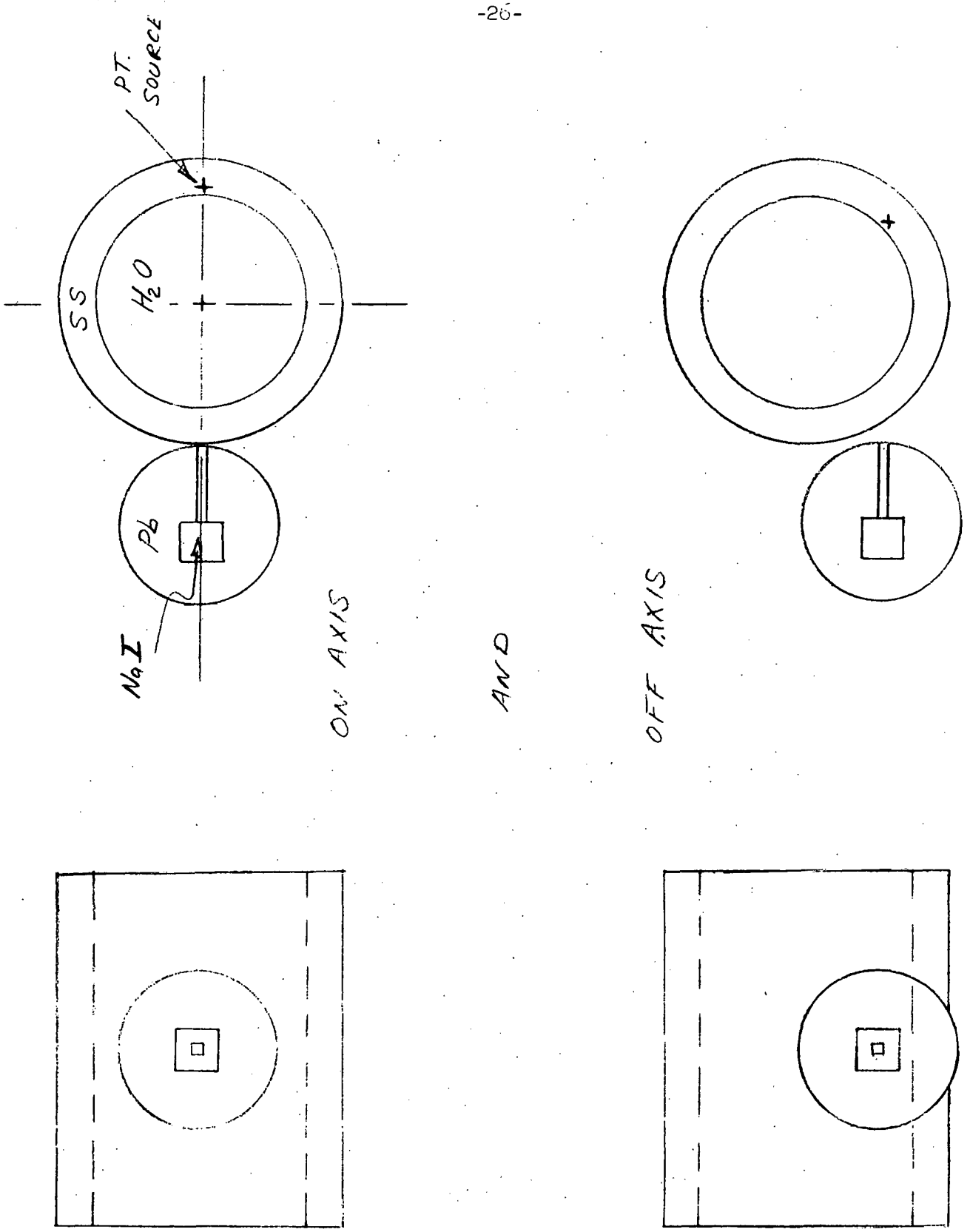

Figure 11. Possible SANDYL geometries for more accurate modeling with variable offset.

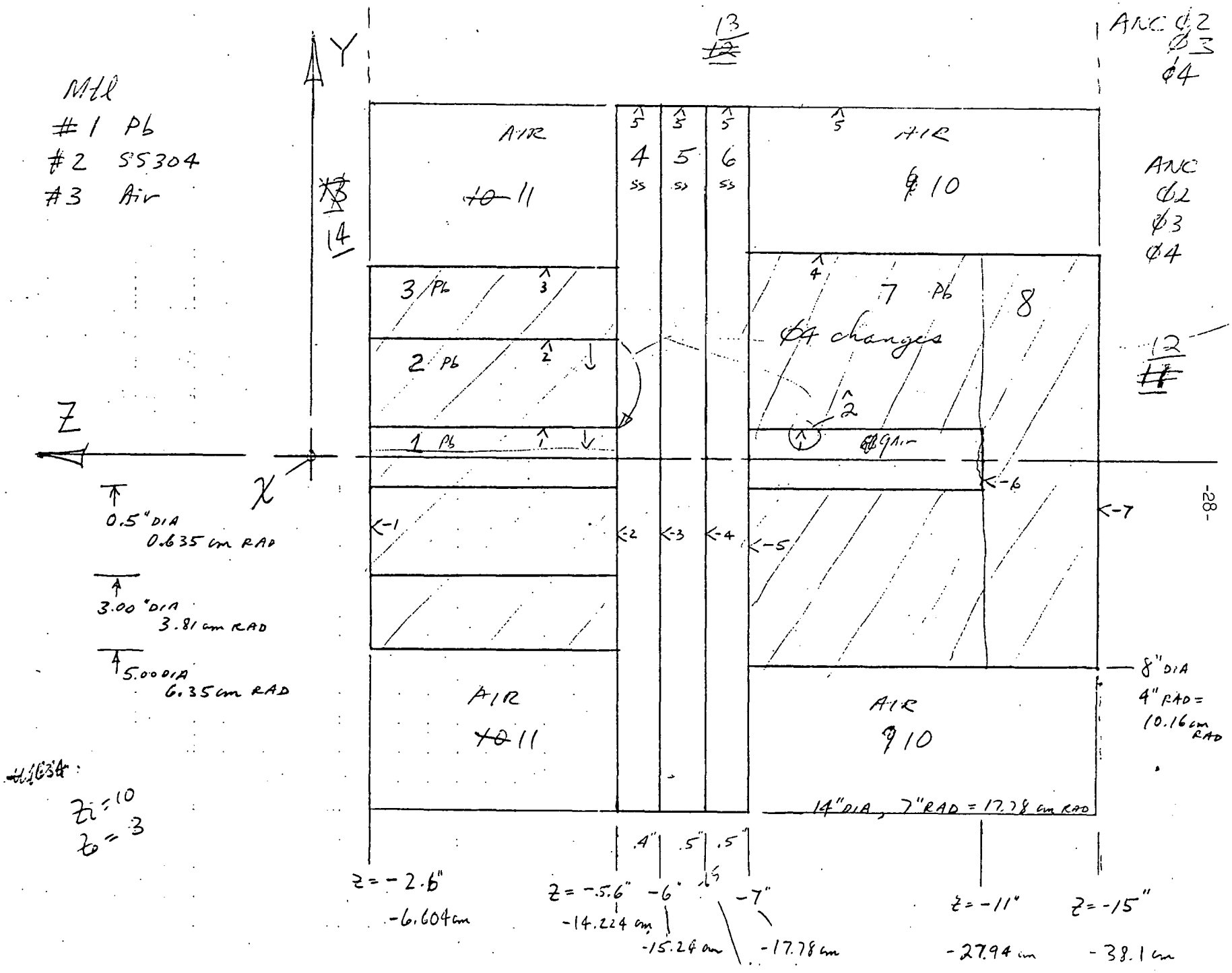
Mtl
#1 Pb
#2 SS304
#3 Air
Y
Z
X
13
14
ANC ∅2
∅3
∅4
AIR
10 11
3 Pb
2 Pb
1 Pb
4 SS
5 SS
6 SS
7 Pb
8
∅4 changes
∅ air
10
-1
-2
-3
-4
-5
-6
-7
0.5" DIA
0.635 cm RAD
3.00" DIA
3.81 cm RAD
5.00 DIA
6.35 cm RAD
8" DIA
4" RAD =
10.16 cm RAD
14" DIA, 7" RAD = 17.78 cm RAD
.4"
.5"
.5"
z = -2.6"
-6.604 cm
z = -5.6"
-14.224 cm
-6"
-15.24 cm
-7"
-17.78 cm
z = -11"
-27.94 cm
z = -15"
-38.1 cm
-28-

NMX
#
1 Pb
2 SS 304
3 air
4 Ge
5 fluid

10 inside zones
3 outside "

ANC ϕ5
ANC ϕ8

ANC ϕ5
ϕ8

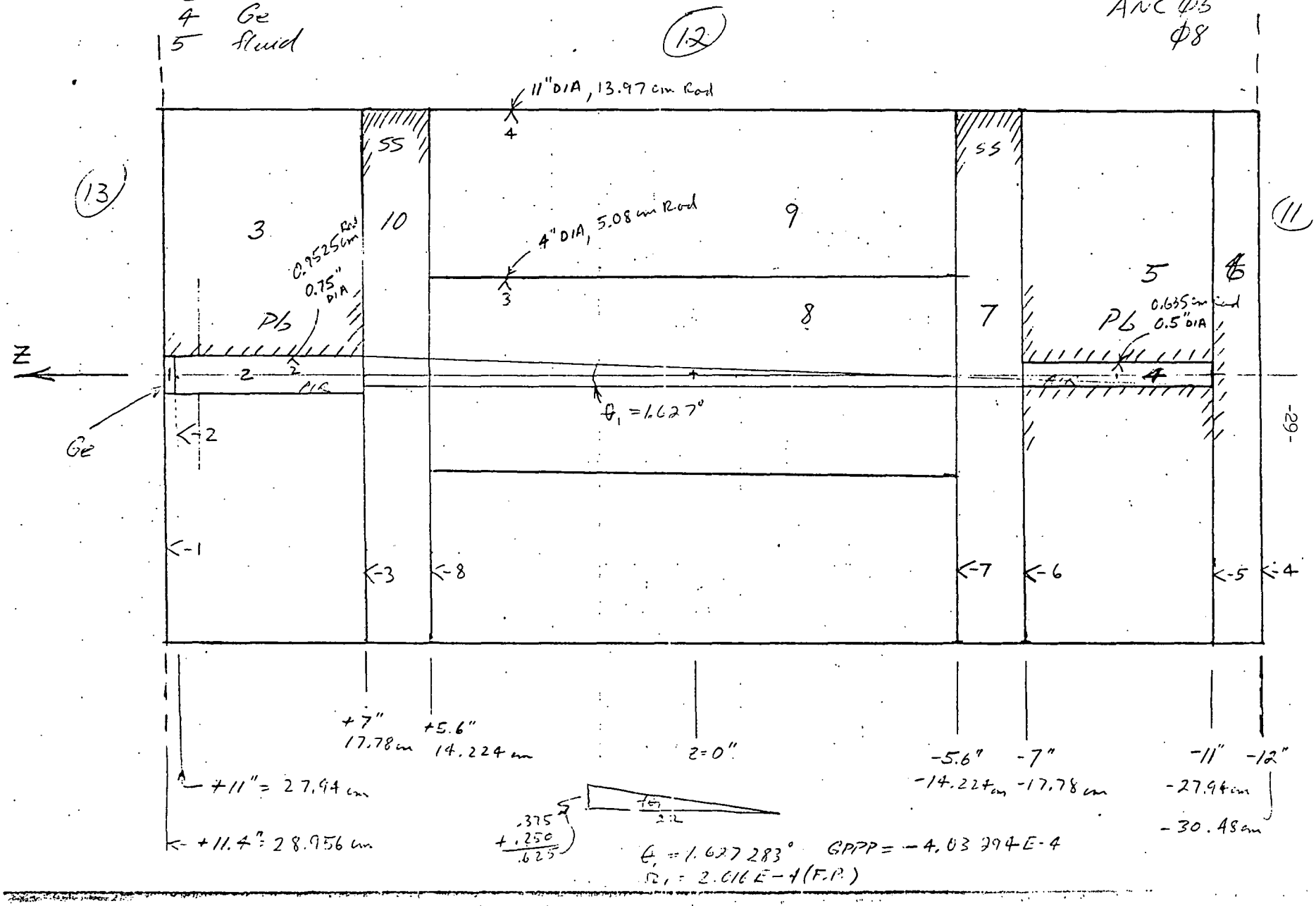

Mtl
#
1 Pb
2 SS 304
3 air
4 Ge
5 fluid

10 inside zones
3 outside "

~~ANC 05~~
~~ANC 08~~
ANC 15
16

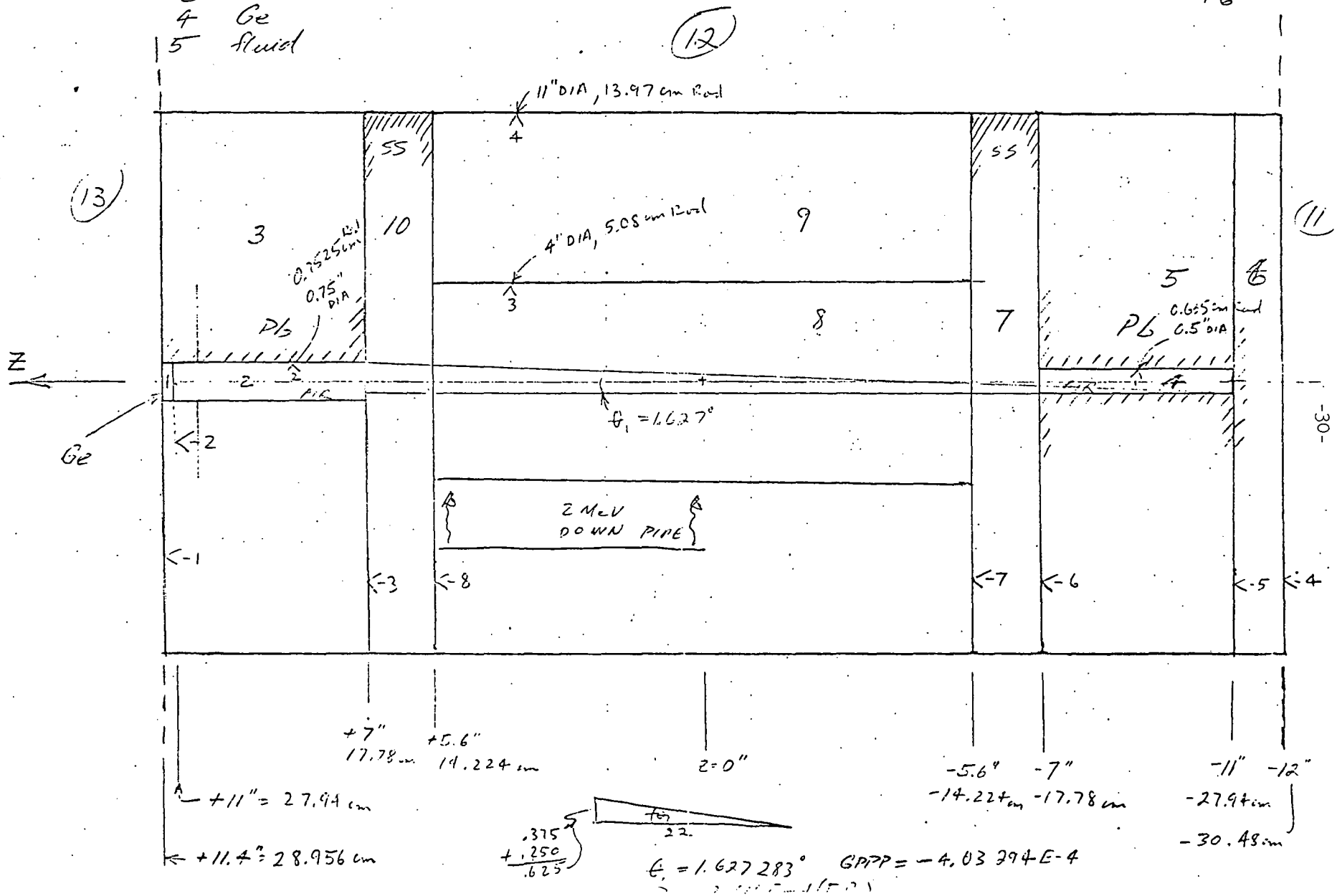

ANC 15
16

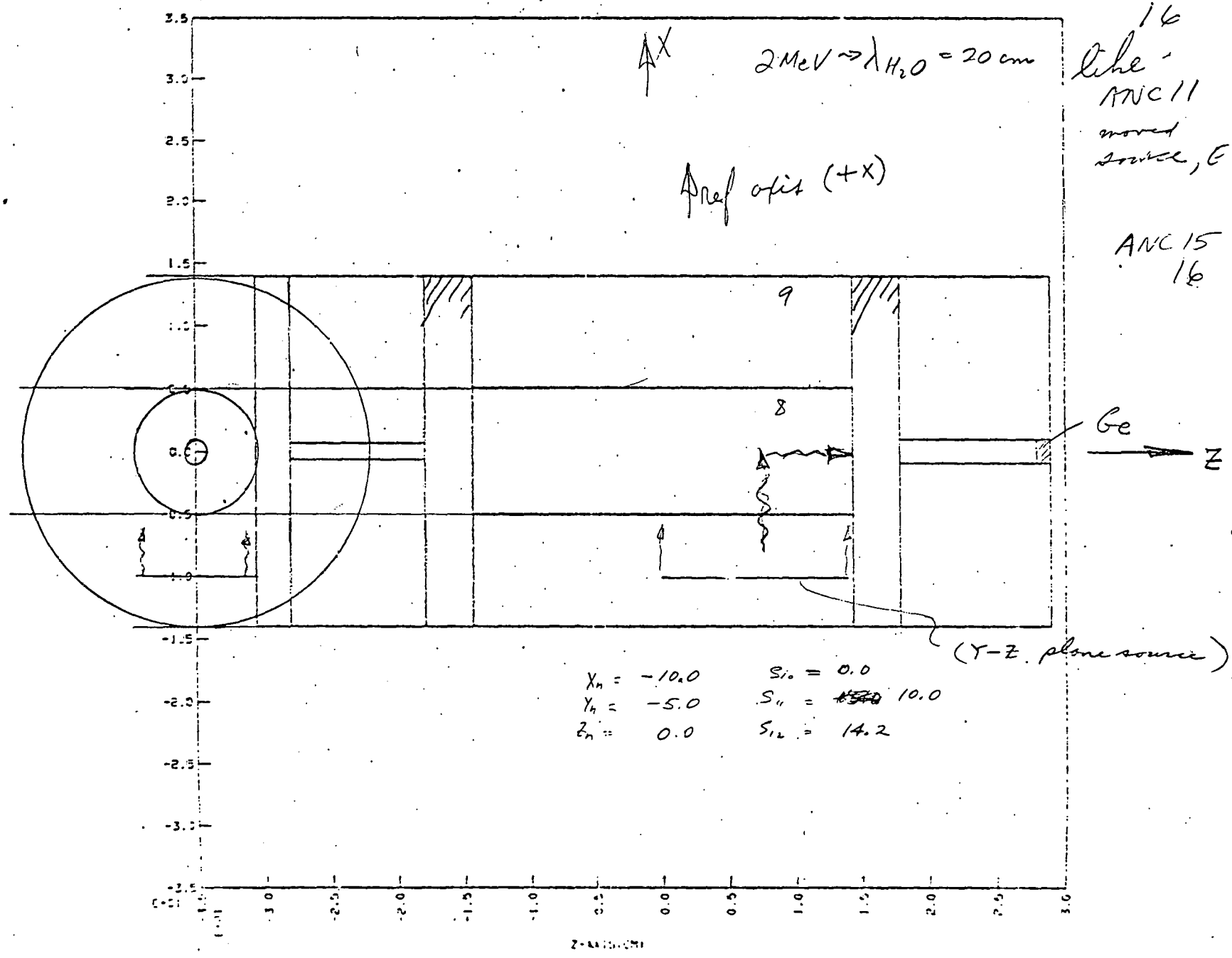

like ANC 11 moved source, E

ANC 15
16

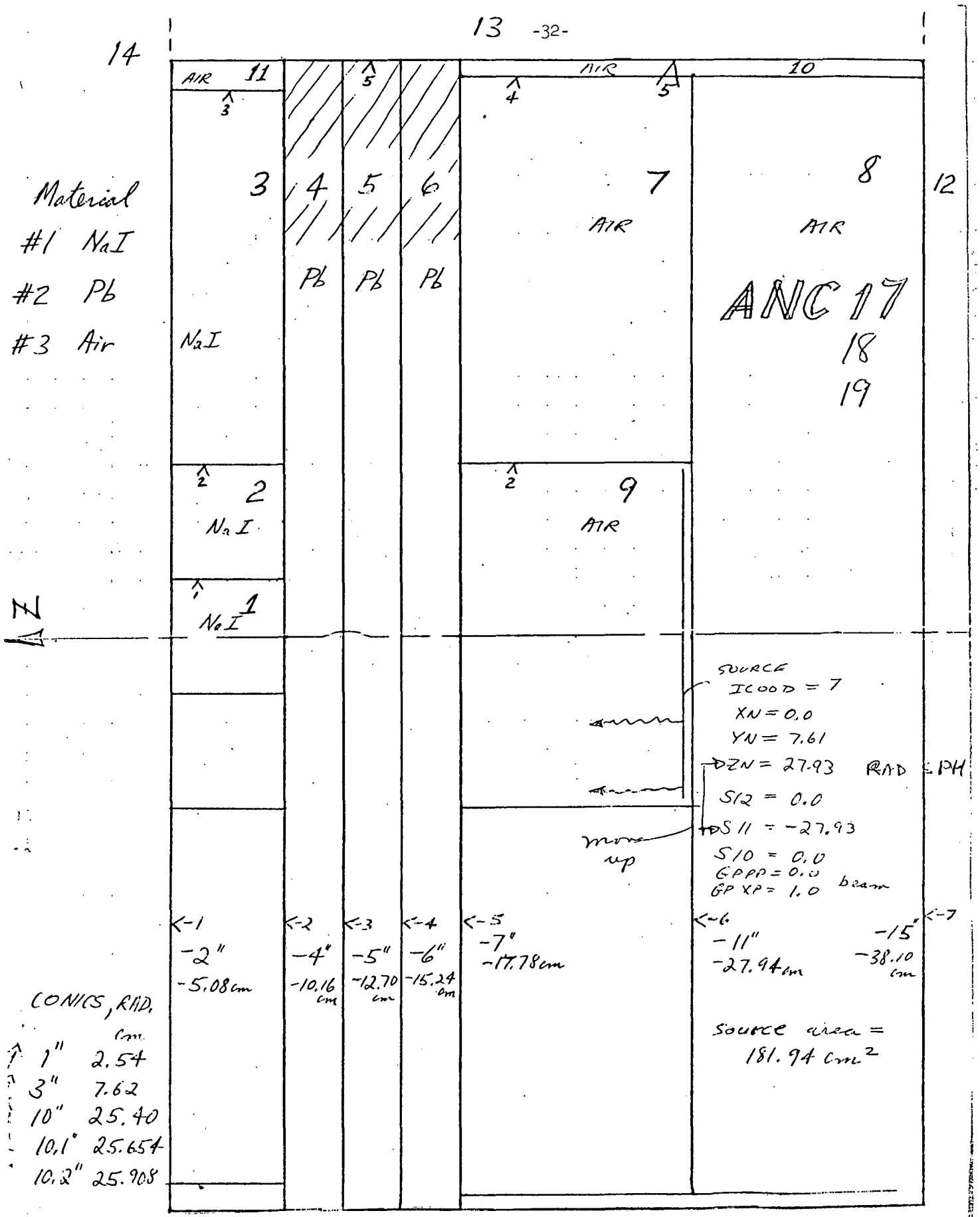
13
14
12
AIR
11
10
3
4
5
6
7
8
9
1
2
Material
#1 NaI
#2 Pb
#3 Air
NaI
Pb
AIR
ANC 17
18
19
N
SOURCE
ICOOD = 7
XN = 0.0
YN = 7.61
DZN = 27.93
RAD
SPH
SI2 = 0.0
SI1 = -27.93
SI0 = 0.0
GPPP = 0.0
GP XP = 1.0
beam
move up
<-1
-2"
-5.08cm
<-2
-4"
-10.16 cm
<-3
-5"
-12.70 cm
<-4
-6"
-15.24 cm
<-5
-7"
-17.78cm
<-6
-11"
-27.94cm
-15"
-38.10 cm
<-7
CONICS, RAD.
cm
1" 2.54
3" 7.62
10" 25.40
10.1" 25.654
10.2" 25.908
source area =
181.94 cm²

DISTRIBUTION

Internal

G. A. Armantrout	L-156	
L. L. Cleland	L-156	
E. A. Lafranchi	L-151	
S. P. Swierkowski	L-156	(10)
R. Wichner	L-156	
TID	L-9	(15)
TIC		(27)

External

A. E. Arave
Aerojet Nuclear Co.
550 2nd Street
Idaho Falls, Idaho 83401

F. Carten
Allied Chemical
550 2nd Street
Idaho Falls, Idaho 83401

R. L. Crumley
Aerojet Nuclear Co.
550 2nd Street
Idaho Falls, Idaho 83401

R. L. Heath
Aerojet Nuclear Co.
550 2nd Street
Idaho Falls, Idaho 83401

A. Stephens
Aerojet Nuclear Co.
550 2nd Street
Idaho Falls, Idaho 83401

R. Wesley
Aerojet Nuclear Co.
550 2nd Street
Idaho Falls, Idaho 83401

Printed in the United States of America
Available from
National Technical Information Service
U. S. Department of Commerce
5285 Port Royal Road
Springfield, Virginia 22151
Price: Printed Copy $___*; Microfiche $2.25

*Pages	NTIS Selling Price
1-50	$4.00
51-150	$5.45
151-325	$7.60
326-500	$10.60
501-1000	$13.60

Technical Information Department
LAWRENCE LIVERMORE LABORATORY
University of California | Livermore, California | 94550